Contemporary crustal movements in California are concentrated within a plate-boundary deformation zone that is typically 50 to 200 km wide, centered approximately on the San Andreas fault. Observations of coseismic, postseismic, and interseismic movements define the earthquake deformation cycle and constrain models of strain accumulation and release for strike-slip plate boundaries.

7. PRESENT-DAY CRUSTAL MOVEMENTS AND THE MECHANICS OF CYCLIC DEFORMATION

By WAYNE THATCHER

CONTENTS

INTRODUCTION

Crustal movements measured in California today sample deformation processes that have continued through at least the past 5 Ma of Pliocene, Pleistocene, and Holocene time. During this interval, several hundred kilometers of right-lateral offset has accumulated across the San Andreas fault system, and many thousands of great earthquakes similar to the historical events of 1857 and 1906 have undoubtedly occurred. The observed deformation results from relative right-lateral translation of the Pacific and North American plates far from the main plate-boundary faults, which are either freely slipping and without major seismic activity, or are in locked frictional contact and slip episodically in repeated great earthquakes. Aseismic fault slip (creep), as occurs across the San Andreas fault in central California (fig. 7.1), causes no crustal deformation beyond a growing offset across the fault, although this offset may be distributed across a zone as broad as a few tens or hundreds of meters. Where the plate-boundary fault is alternately locked aseismically in its upper 10 km or so and abruptly slipping in great earthquakes, deformation extends several tens of kilometers into the plate interiors. Between large events, elastic strains build up in this zone and are episodically released every few hundred years. Subsequent postearthquake recovery processes redistribute the strains aseismically for years to decades after a major shock, and this deformation gradually merges into the steady accumulation of elastic-strain energy that persists until the frictional strength of the fault is again exceeded. This sequence of interearthquake strain accumulation, coseismic strain release, and postseismic readjustment is thus a recurring process, here referred to inclusively as the earthquake deformation cycle.

Several fault-zone features result in measurable deformation spread over an extremely broad plate-boundary zone. This deformation occurs where the San Andreas fault system comprises several subparallel splays, as in both the San Francisco Bay region and southern California. There, both aseismic slip and major strike-slip

◀ FIGURE 7.1.—A wall and sidewalk in Hollister, Calif., are bent and offset by creep on the Calaveras fault. A slip rate of 5 to 6 mm/yr characterizes much of the Calaveras fault. View eastward along north side of Sixth Street. Photograph by R.E. Wallace, U.S. Geological Survey.

earthquakes have been documented, some on the same fault strand, and the entire zone of plate-boundary deformation is exceptionally broad. Major changes in fault strike also play a role in redistributing plate-boundary deformation and diffusing it over a wider zone. Compressional bends introduce uplift, crustal thickening, and subsidiary reverse faulting, such as in the Transverse Ranges of southern California. Extensional bends are characterized by subsidence, basin filling, and, possibly, volcanism, as occurs in the Imperial Valley. Extensional and compressional features are more localized at the smaller-scale discontinuities and changes in fault strike that occur throughout the San Andreas system.

Crustal movements observed at the surface reflect deformation processes occurring at depth in the lithosphere. Both laboratory rock-mechanics experiments and studies of exhumed fault zones define the nature of these processes, which, in turn, constrain the classes of large-scale faulting models consistent with surface measurements. In the cool and brittle seismically active parts of the crust, elastic processes are dominant, the frictional strength of active faults increases linearly with depth, and faulting is controlled by Coulomb failure. The transition from brittle seismic behavior to ductile aseismic deformation occurs in the midcrust. Although it is generally agreed that this transition occurs as a result of increasing temperature, its precise mechanism is uncertain. If deformation in the midcrust is concentrated within a narrow vertical shear zone lying beneath the seismically active fault plane, then the brittle/ductile transition may reflect either the increasing importance of ductile or cataclastic flow at depth (Sibson, 1982) or a thermally controlled transition from unstable to stable frictional sliding (Brace and Byerlee, 1966; Tse and Rice, 1986). However, if ductile deformation is broadly distributed in the midcrust, then the cyclic buildup and relief of stresses in the brittle seismogenic crust is controlled by the stress transfer between the elastic lithosphere and ductile "asthenosphere" and the flow properties of the latter.

Both the steady, aseismic movements within the San Andreas plate-boundary zone and the coseismic strain release in large earthquakes are well within the range of detectability of repeated geodetic-survey measurements. The purpose of this chapter is to summarize the salient features of these observations, demonstrating the constraints they place on the amount of present-day plate motion occurring across the San Andreas plate-boundary zone and showing how measurements shed light on the mechanics of the cycle of strain accumulation and release. The emphasis is necessarily on movements close to the main strands of the San Andreas fault system, where observations are most numerous, although some networks extend as far as 100 km from the major faults. The measurements include triangulation, repeated observations of the angular separation of permanent survey markers, for which useful data date back to about 1850, when gold was first discovered in California; trilateration, repeated line-length measurements made by laser ranging since about 1970; and local measurements of aseismic fault slip made periodically or recorded continuously over apertures of about 10 to 100 m since about 1960.

OBSERVATIONS OF CRUSTAL DEFORMATION

The focus here is on the spatial and temporal patterns of interearthquake horizontal crustal movements in California that owe their origins to relative motion between the Pacific and North American plates, movements that supply the strain energy which is stored in crustal rocks and ultimately released in large shallow-focus earthquakes. Observations of purely coseismic crustal deformation are not explicitly considered in this chapter; such movements are now well-understood consequences of slip on approximately the upper 10 to 15 km of vertical strike-slip faults. These models and their predicted deformation patterns are discussed within the context of the entire earthquake deformation cycle in the next section. Readers interested in the coseismic movements observed for specific San Andreas earthquakes are referred to the reports by Lawson (1908) and Thatcher (1975) (1906 San Francisco earthquake), Zhang and others (1988) (1940 El Centro earthquake), and Segall and Harris (1987) (1966 Parkfield earthquake).

Vertical crustal movements can locally be substantial, at least when averaged over recent geologic time (see Yeats, 1977; Lajoie, 1986). Deformation from reverse-faulting earthquakes has also been well documented in several events (for example, 1952 Kern County earthquake by Stein and Thatcher, 1981; 1971 San Fernando earthquake by Castle and others, 1975; 1983 Coalinga earthquake by Stein, 1983). Nonetheless, vertical movements are second-order features along most of the San Andreas fault system, and so they are not considered further in this chapter.

Furthermore, in this chapter there is no review of measurement techniques, methods of analyzing and reducing data, or the mathematical and computational tools used in modeling deformation processes. Interested readers are referred to the reports by Bomford (1980) and Savage and Prescott (1973) for descriptions of horizontal-deformation-surveying methods and their precision, to those by Prescott (1976, 1981), Thatcher (1979), and Segall and Harris (1987) for discussions of data-analysis methods, and to the references cited below in the section entitled "Mechanics of Deformation" for details of the mathematical techniques used in model formulation.

Horizontal interearthquake deformation is summarized below in rates of both displacement and shear strain. For both of these parameters, the components parallel to major active faults are the most significant and best illustrate the dominant pattern of present-day tectonic movements, and so in this chapter these components are commonly shown exclusively. For example, although three independent tensor components are needed to completely characterize the horizontal-deformation field, in California the only significantly nonzero strain-rate component is commonly the shear strain parallel to the local trend of faults in the San Andreas system. Here, I consider only the component of maximum horizontal shear-strain rate, which, within observational uncertainty, almost invariably parallels the San Andreas fault or one of its major strands.

SHEAR STRAIN ON THE SAN ANDREAS FAULT SYSTEM

Rates of contemporary shear strain are displayed in several complementary ways in figures 7.2 through 7.4; details of each rate determination are summarized in table 7.1. Although only the magnitude of the maximum shear-strain rate is shown in each figure, the orientation of the maximum-horizontal-contraction axis is listed in table 7.1. Note that for each of the strain rates shown in figures 7.2 through 7.4, aseismic fault slip contributes only negligibly, if at all, to the measured deformation. Further details on each strain field determination can be found in the references cited in table 7.1.

Shear-strain rates peak at 0.4 to 0.6 μrad/yr (fig. 7.2) across the currently locked northern and southern sections of the San Andreas fault. Significant but slightly lower strain rates of 0.3 to 0.4 μrad/yr are observed across right-lateral strike-slip faults in the northern California Coast Ranges (north of lat 38° N.) east of the San Andreas fault, as well as across the San Jacinto fault in southern California. Shear-strain rates resolvably greater than zero are observed as far as about 80 km from the San Andreas fault itself.

In addition, significant deformation is occurring across active faults in east-central California. In the White Mountains, along the southern California-Nevada State line, small but resolvable strain rates (0.06 ± 0.02 μrad/yr) have been measured, and the orientation of the strain field indicates crustal extension perpendicular to north-south-striking normal faults in the area. Somewhat higher deformation rates are observed farther south, where right-lateral strain is occurring parallel to the Owens Valley fault, site of the $M \simeq 8$ earthquake of 1872 (see chap. 6).

Shear-strain rate is plotted as a function of perpendicular distance from the San Andreas fault in figure 7.3. Deformation rates peak at the fault and decrease to half their maximums at a distance of about 30 km from the fault. Most of the deformation is encompassed within a zone about 100 km wide centered on the fault ("San Andreas boundary deformation zone"), as discussed below. However, the reader may confirm that this total lies in the range of about 30–40 mm/yr by drawing a smooth curve through the data plotted in figure 7.3 and integrating this curve (that is, measuring and summing the total area underneath the curve) from –60 to +60 km.

Maximum shear-strain rates at the San Andreas fault tend to be higher across the 1906 earthquake rupture in northern California (approx 0.6 μrad/yr) than in southern California (0.4 μrad/yr), although the Carrizo Plain data violate this generalization. Rather high deformation rates are also observed 20 to 60 km east of the San Andreas fault in the northern California Coast Ranges.

Shear-strain rates at various locations on the two currently locked sections of the San Andreas fault are plotted versus time since the most recent great earthquake at each locality in figure 7.4. Most of these data are derived from triangulation measurements, many of which were first made in the late 19th or early 20th century. Thus, these determinations are much less precise than those listed in table 7.1 and plotted in figures 7.2 and 7.3, most of which are from the post-1970 period. Nonetheless, it is clear from figure 7.4 that deformation rates on the fault are much higher in the years to tens of years immediately after a great earthquake than they are later. Although it may be questionable to lump values from northern and southern California together on a single plot, the temporal decline in shear-strain rate shown in figure 7.4 depends only on about the first 70 years of data plotted, all of which come from the 1906 rupture on the northern section of the San Andreas fault.

ASEISMIC SLIP, INTEGRATED DISPLACEMENT RATES, AND PACIFIC-NORTH AMERICAN PLATE MOTION

Rates of surface aseismic slip (fault creep) at representative points on the San Andreas fault system are listed in table 7.2 and plotted in figure 7.5. All fault segments displaying measurable aseismic slip are represented, but the detailed distribution along each segment is not shown; interested readers are referred to the references cited in table 7.2 for more details. Figure 7.5 also displays the rates of relative right-lateral displacement integrated across geodetic networks of 50- to 140-km aperture that span the San Andreas and related faults in seven areas of California, for several of which the detailed displacement-rate pattern is shown in figures 7.6 and 7.7.

With the notable exception of the central, creeping section of the San Andreas fault, aseismic slip at the surface represents only a very small proportion of the

total right-lateral displacement across the San Andreas fault system. On the 160-km-long central section of the San Andreas fault, maximum fault-creep rates average 30 mm/yr, close to the geodetically derived displacement rate of 33±1 mm/yr obtained over a 60-km aperture that spans the fault and the California Coast Ranges to the southwest. These data are the strongest evidence that no significant strain is accumulating in the crustal blocks adjacent to the fault in this region, and so all the relative plate motion taken up by the San Andreas system is here being accommodated by rigid-block translation across the fault. Just north of this segment, on the southern section of the Calaveras fault, a significant amount of right-lateral slip at a rate of about 13 mm/yr, occurs as fault creep. Elsewhere in California, however, measured aseismic-slip rates range from 2 to 6 mm/yr, and creep

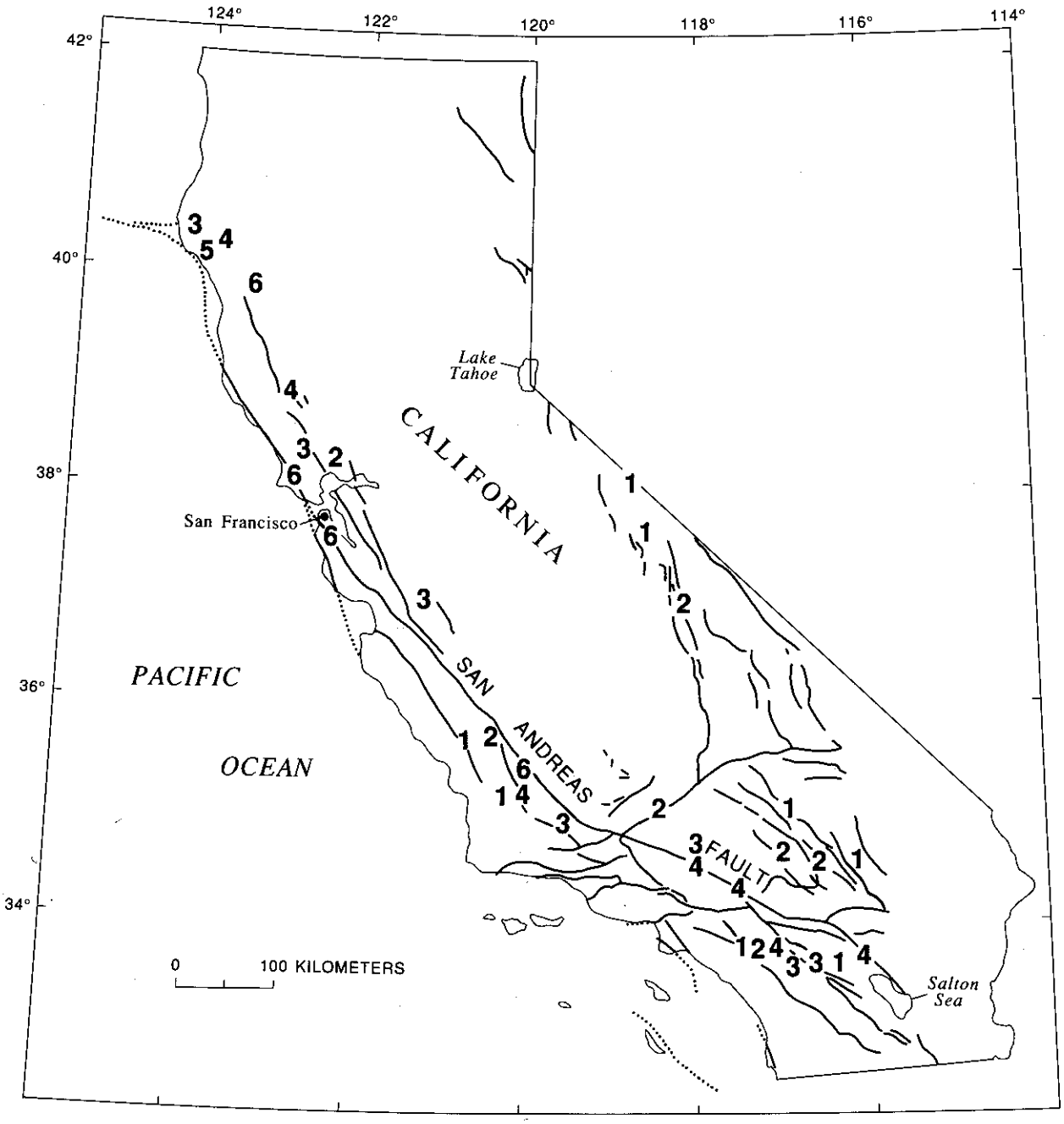

FIGURE 7.2.—Shear-strain rates (in 10^{-7} rad/yr) and major active Quaternary faults of California; faults dotted where concealed. See table 7.1 for details.

commonly occurs only on restricted segments of otherwise-locked faults (for example, the Garlock and San Jacinto faults).

The integrated right-lateral displacement rates shown in figure 7.5 firmly constrain the proportion of Pacific-North American relative plate motion accommodated across the San Andreas fault system in California. In northern, central, and southern California, maximum rates range from 33 to 37 mm/yr. Global reconstructions of the motions of the major tectonic plates over the past 3 Ma, as well as analyses of magnetic-anomaly lineations at the mouth of the Gulf of California, point to a relative Pacific-North American plate-motion rate of 49±3 mm/yr (DeMets and others, 1987). The San Andreas fault system thus accounts for 70 to 80 percent of the relative plate motion, although the San Andreas fault itself does not everywhere take up all of this motion, and deformation is typically distributed across a boundary zone about 100 km wide.

Precisely how much additional relative plate motion is accommodated across other faults in California is uncertain, although the amount is probably very little. According to Minster and Jordan (1987), very long baseline interferometric (VLBI) surveying results indicate that oblique extension of the Basin and Range province, directly east of California, is occurring at a rate of 10±2 mm/yr with an orientation of N. 56° ±10° W. Depending on the exact rate and orientation of this extension, as well as on the precise direction of relative Pacific-North American plate motion, the residual "missing" plate motion being accommodated in California on faults other than those of the San Andreas system ranges from negligibly small to possibly as much as 10 mm/yr. Thus, although the geodetic coverage in California is far from complete (see figs. 7.2, 7.5), all or most of the zone of significant plate-boundary deformation apparently has been encompassed.

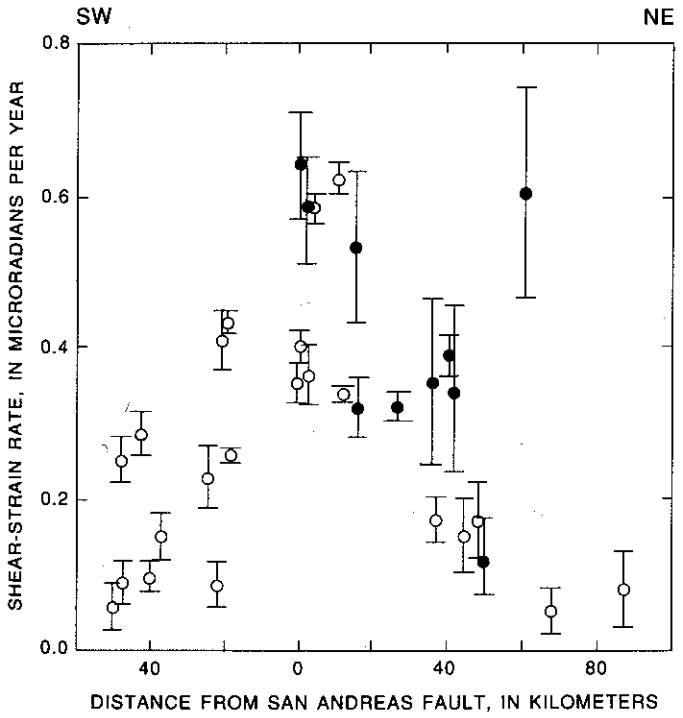

FIGURE 7.3.—Shear-strain rate versus perpendicular distance from the San Andreas fault. Dot, determination from northern California; circle, determination from southern California. 1-σ error bars shown for reference.

DETAILED DISPLACEMENT-RATE PATTERNS

Considerable detail on the distribution of deformation in the San Andreas boundary zone is provided by the rather complete geodetic coverage available in the San Francisco Bay region and southern California. In the method used to reduce these data, geodetic-line-length changes are used to determine station-displacement rates relative to a point at the center of gravity of the network. Fault-normal displacements are permitted by this method, but their values are minimized in the inversion

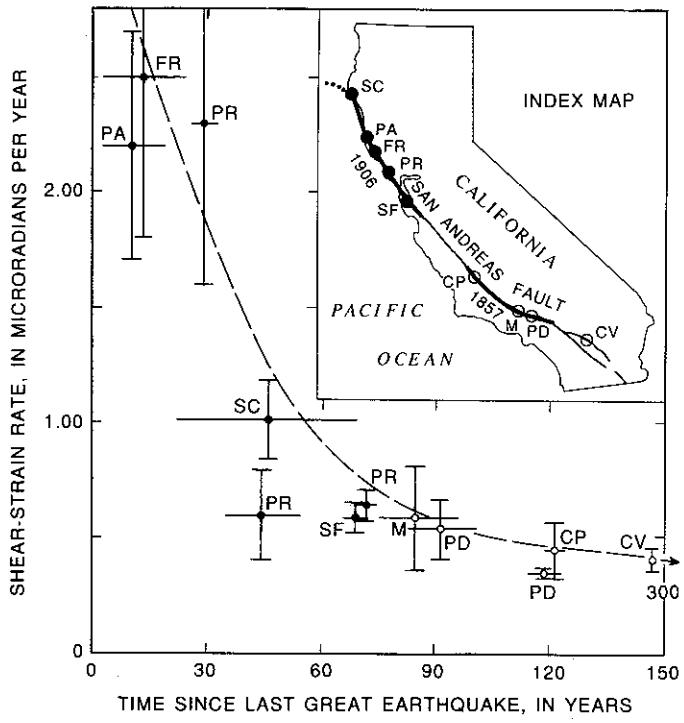

FIGURE 7.4.—Shear-strain rate versus time since last great earthquake (years 1906 and 1857 in inset; heavy line indicates extent of fault rupture) on the San Andreas fault. CP, Carrizo Plain; CV, Coachella Valley; FR, Fort Ross; M, Mojave; PA, Point Arena; PD, Palmdale; PR, Point Reyes; SC, Shelter Cove; SF, San Francisco. Locations of data points are keyed to index map. For each data point, vertical bar is 1 σ, and horizontal line indicates time interval between surveys. Data points are plotted at middle of intervals. Dots, determinations from northern California; circles, determinations from southern California; dashed curve, approximate fit to data (Thatcher, 1983).

TABLE 7.1.—*Shear-strain rates in California*

[Maximum compression measured from north, with clockwise direction positive]

Area	Location		Rate (ppm/yr)	Maximum compression direction* (°)	Interval	Reference
	Lat N.	Long W.				
Mendocino	40.1°	124.0°	0.53±0.10	3±4	1981–84	Breen and others (1987).
	40.1°	123.7°	.35±0.11	11±6	--	
	40.2°	124.1°	.34±0.11	21±9		
Round Valley	39.9°	123.3°	.60±0.14	-11±5	1942–64	Prescott (1985).
Point Reyes	38.1°	122.8°	.64±0.07	2±2	1972–82	Prescott and Yu (1986).
Santa Rosa (Rodgers Creek fault).	38.4°	122.8°	.32±0.02	12±2	--	--
The Geysers (Maacama fault).	38.8°	122.9°	.39±0.03	11±3	--	--
Napa (West Napa fault)	38.3°	122.3°	.17±0.05	20±9	--	--
San Francisco peninsula	38.5°	122.4°	.58±0.07	-2±9	1970–80	Prescott and others (1981).
White Mountains	37.9°	118.6°	.06±0.02	-13±12	1972–79	Savage and Lisowski (1984).
	37.5°	118.5°	.06±0.02	-8±14		
Owens Valley	36.9°	118.1°	.16±0.06	28±12	1974–79	Savage and Lisowski (1980).
Hollister (E. of Calaveras fault).	36.9°	121.3°	.32±0.04	-16±3	1971–78	Savage and others (1979).
San Luis network:						
Central	35.5°	120.4°	.23±0.04	-23±3	1977–83	N.E. King (unpub. data, 1988).
West	35.4°	120.7°	.09±0.03	-18±10	--	--
Carrizo network:						
A	35.4°	119.8°	.62±0.02	--	1977–83	N.E. King (unpub. data, 1983).
B	35.3°	119.8°	.58±0.02	--	--	--
C	35.1°	119.9°	.43±0.02	--	--	--
D	35.1°	120.2°	.10±0.02	--	--	--
Tehachapi network:						
Garlock fault	34.9°	118.5°	.17±.03	4±3	1973–83	King and Savage (1984).
San Andreas fault	34.6°	118.0°	.34±.01	-17±1	--	--
Cajon network	34.3°	117.5°	.36±.04	-16±2	1974–84	Savage and others (1986).
Los Padres network	34.8°	119.5°	.26±.01	-1±1	--	
Barstow	35.0°	116.9°	.08±.05	24±17	1979–84	King (1985).
Palmdale	34.4°	118.2°	.35±.03	-19±4	1971–80	Savage and others (1981).
Mojave network:						
W1	34.6°	117.0°	.17±.05	4±11	1934–82	Sauber and others (1986).
W3	34.4°	116.6°	.15±.05	5±8	--	--
Eastern	34.5°	116.1°	.05±.03	--	--	--
Anza network:						
A	33.8°	117.4°	.06±.03	--	1973-81	King and Savage (1983).
B	33.8°	117.1°	.15±.03	30±13	--	--
C	33.8°	117.0°	.41±.04	21±5	--	--
D	33.5°	116.8°	.25±.03	30±8	--	--
E	33.5°	116.7°	.29±.03	1±5	--	--
F	33.6°	116.4°	.09±.03	--	--	--
G	33.7°	116.1°	.40±.02	8±2	--	--

process (see Prescott, 1981). Gross departures from this constraint would be revealed by notable disagreements between observed and predicted line-length changes, but no such discrepancies were found for the results presented here. Because the fault-normal displacement rates are small and show no consistent trends, they are not plotted on the profiles presented here.

Displacement rates in the San Francisco Bay region are plotted in figure 7.6. The distribution of deformation varies considerably across the San Andreas boundary zone from north to south of the San Francisco Bay. In the north bay, the integrated right-lateral-displacement rate across the network of 27±3 mm/yr (fig. 7.6*B*) indicates that not all of the boundary zone has been captured within its 110-km aperture. Within about 5 km of the San Andreas fault, rapid change in the gradient of deformation rate indicates that interearthquake strain is concentrated close to the fault. Outside this near-fault region, deformation southwest of the fault appears to be negligible. Northeast of the fault, however, the persistence of significant movements right to the edge of the profile suggests that the 5- to 10-mm/yr deficit in boundary-zone deformation across this profile is being accommodated to the east of the Green Valley fault. Across the central and south bay (fig. 7.6*C*), movements are more evenly distributed through the network, and the integrated

TABLE 7.2.—*Representative aseismic-slip rates on faults of the San Andreas system*

Fault	Site	Lat N.	Long W.	Rate (mm/yr)	Reference
Hayward	Hayward network	37.6°	122.1°	6	Prescott and Lisowski (1983).
Northern section of the Calaveras.	Camp Parks	37.7°	121.9°	3	Do.
Southern section of the Calaveras.	San Felipe	37.0°	121.5°	13	Lisowski and Prescott (1981).
San Andreas	Cienega Winery	36.7°	121.5°	13	Schulz and others (1982).
Do	Eade Ranch	36.4°	121.0°	30	Buford and Harsh (1980).
Do	Parkfield (Durham Ranch)	35.9°	120.4°	13	Do.
Garlock	Cameron	35.1°	118.3°	4	Louie and others (1985).
San Andreas	Indio Hills	33.7°	116.2°	2	Do.
San Jacinto (Coyote Creek strand).	Bailey's Well	33.0°	116.0°	5	Do.
Imperial	Interstate Highway 80	32.8°	115.5°	5	Do.

displacement rate of 37±3 mm/yr across the south bay suggests that the entire boundary zone has been spanned. Closer examination of the profile, however, reveals several zones of locally high deformation gradient, one across the San Andreas fault, where it resembles that observed near the fault in the north bay. In addition, rapid changes in the profile across the Hayward and Calaveras faults reflect aseismic slip at rates of 3 to 6 mm/yr on these faults (see fig. 7.5).

In southern California (fig. 7.7), deformation across the San Andreas boundary zone notably broadens from the Salton Sea, in the south, northwestward to the Big Bend region of the San Andreas fault north of Los Angeles (see fig. 7.5). At the south end of the Salton Sea, all of the boundary-zone deformation, 35±1 mm/yr, occurs within an area about 50 km wide (profile S, fig. 7.7*C*) that rapidly broadens to more than 100 km wide north and west of the Salton Sea (profile N, fig. 7.7*C*) and, possibly, broader still by about 50 km farther northwest (fig. 7.7*B*). North and west of Los Angeles, networks of 100-km aperture capture only 18±2 mm/yr of the total right-lateral-displacement rate (fig. 7.5). The profiles in figures 7.7*B* and 7.7*C* also show that in contrast with the northern section of the San Andreas fault, deformation gradients across the fault are smoother, and deformation is not so closely concentrated near the fault.

MECHANICS OF DEFORMATION

The observations described in the previous section point to a range of mechanical behavior for the faults comprised by the San Andreas system, from freely sliding with only minor accompanying seismicity, to completely locked from the surface to seismogenic depths except for abrupt slip during infrequent great earthquakes.

On the 160-km-long central section of the San Andreas fault, virtually all fault slip occurs aseismically. Slip rates measured at or near the fault are close to the average rate for the entire San Andreas boundary zone (fig. 7.5), no strain is detectable in the crustal blocks adjacent to the fault, and historical earthquakes of $M \geq 5\frac{1}{2}$ have not occurred. Abundant minor seismicity (see fig. 4.10) contributes only negligibly to the slip budget, and except for a few small patches of fault surface that are in frictional contact between these small earthquakes, the first-order steady-state model for this segment involves rigid translation of adjacent fault blocks across the freely sliding plane of the San Andreas.

A transitional behavior applies to those fault segments where steady-state fault creep is observed at the surface but historical or prehistoric earthquakes of $M \geq 6$ have been documented. Examples include the Parkfield and Coachella Valley segments of the San Andreas fault, the Hayward fault, and the Imperial fault. On these segments, during the interseismic phase of the earthquake cycle, the fault is inferred to be freely slipping in its upper few kilometers, in locked frictional contact at seismogenic depths (approx 3–10 km), and once again freely slipping at greater depths (fig. 7.8*A*). The result of this slip distribution is interseismic creep at the surface fault trace and elastic-strain accumulation in the adjacent blocks (figs. 7.8*B*, 7.8*C*).

THICK- AND THIN-LITHOSPHERE MODELS

The most extreme features of locked fault behavior are currently observed on the two San Andreas fault segments where great earthquakes have occurred in historical time, in 1857 and 1906 (see fig. 5.11 for locations and coseismic-slip distributions). On these segments, no aseismic slip is observed at the Earth's surface, the two faces of the fault are in locked frictional contact to depths

of 10 to 15 km, and interearthquake slip is either extremely small or absent. At greater depths, the mechanics of fault movement is uncertain, but two models bound the range of expected behavior (fig. 7.9). In the first, the thick-lithosphere model, the depth D of coseismic faulting is much less than the thickness H of elastically strong lithosphere. Interearthquake deformation then predominantly results from episodic or steady aseismic slip on the downward extension of the seismogenic fault zone, and any effects of the underlying weak asthenosphere can be safely neglected. In the second, the thin-lithosphere model (fig. 7.9), coseismic faulting depth is comparable to elastic-plate thickness. In this model, transient postseismic and steady interseismic flow in the

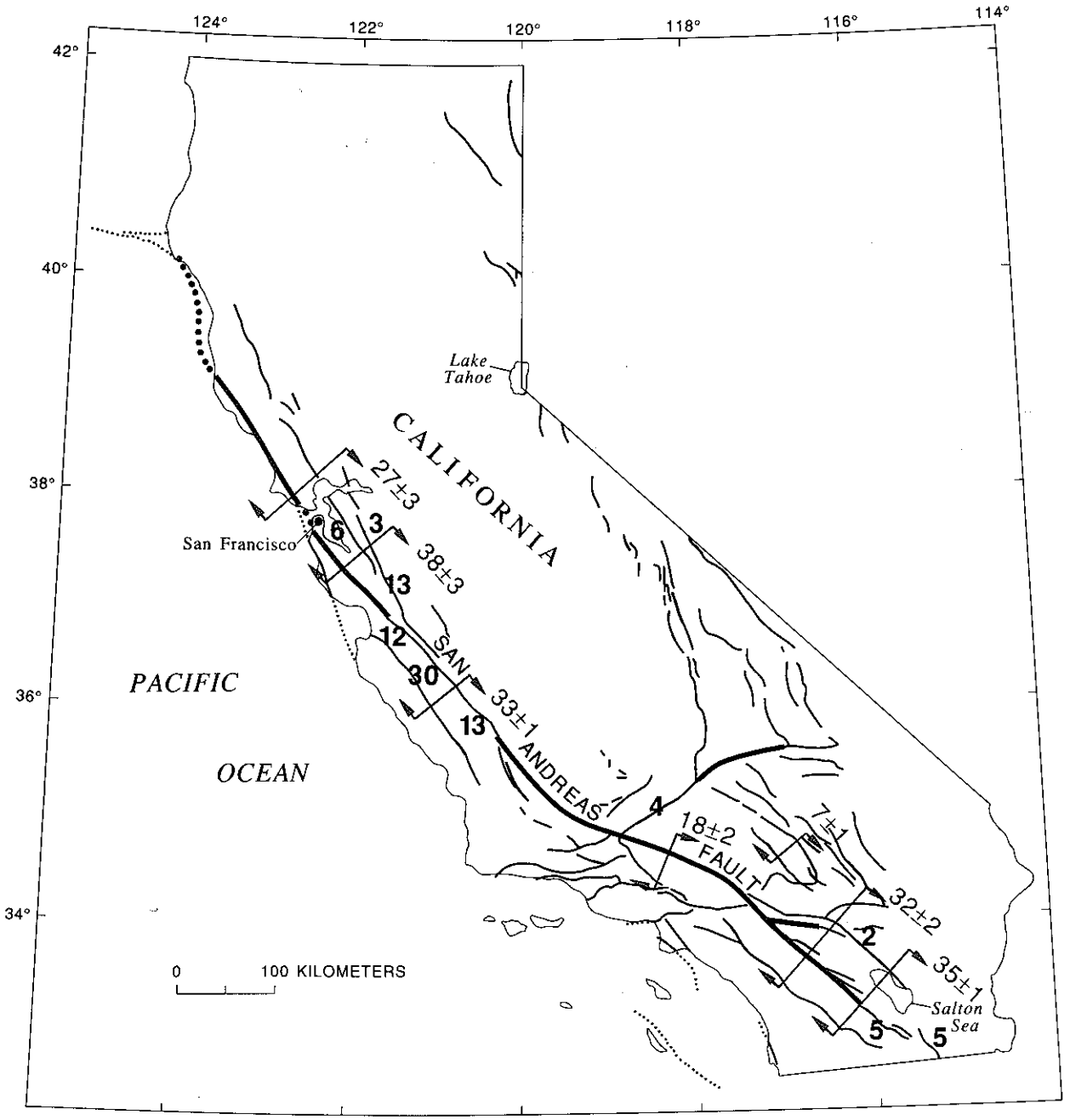

FIGURE 7.5.—Sketch map of California, showing rates (red numbers) of aseismic slip (fault creep) and relative right-lateral-displacement rates (blue numbers) near arrows, which indicate direction of relative movement along major active strands of the San Andreas fault system. Values in millimeters per year. Locked (no surface slip) segment of major fault, red line; other Quaternary fault, black line; faults dotted where concealed. See table 7.2 for details.

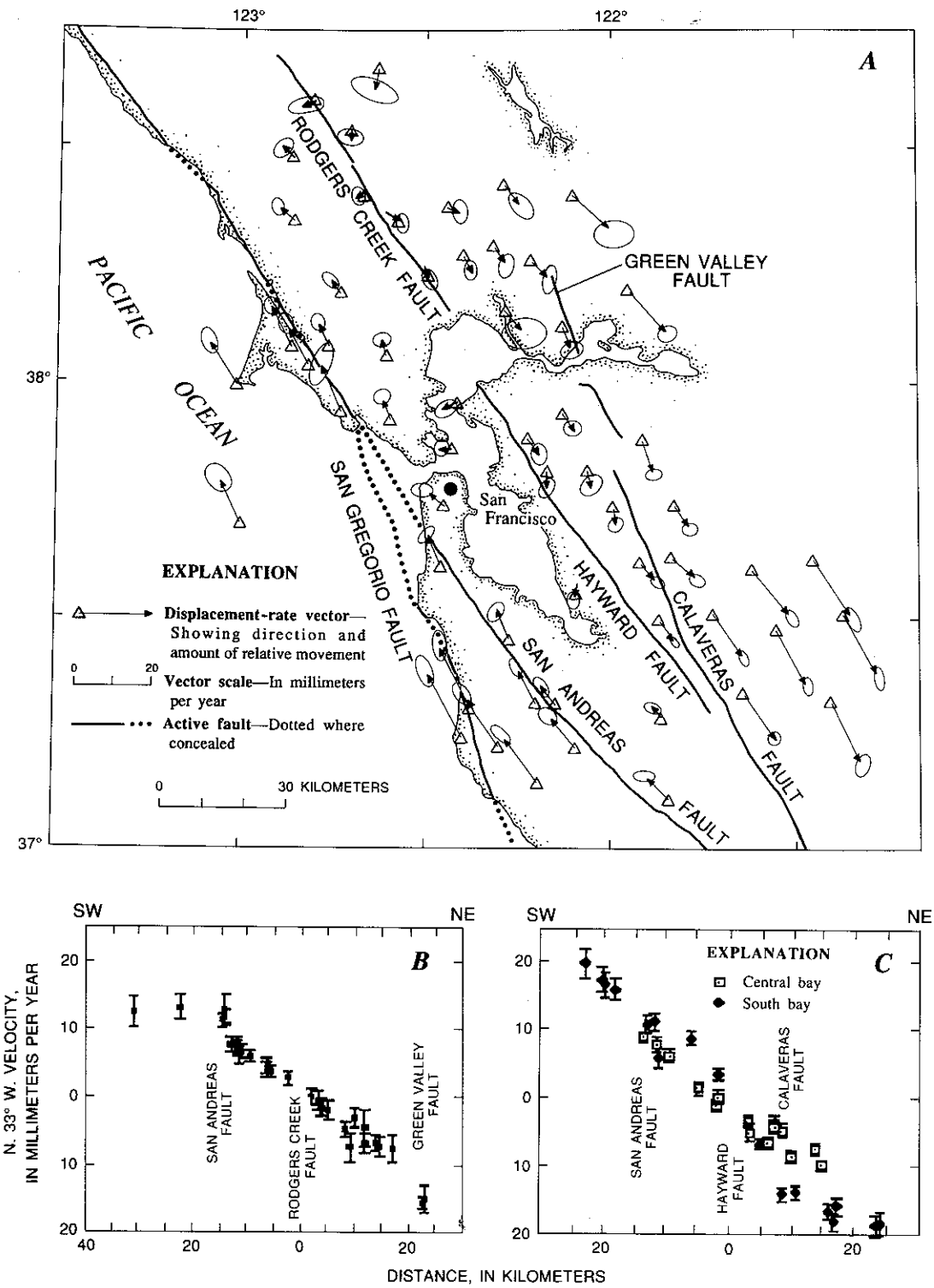

FIGURE 7.6.—Displacement rates across the San Francisco Bay region. *A*, Relative right-lateral displacement rates determined from repeated geodetic surveys made during 1971–87. Error ellipses show 95-percent-confidence limits for each determination (Prescott and others, 1987). *B*, Relative station velocities parallel to approximate trend of the San Andreas fault (N. 33° W.) plotted against distance perpendicular to this trend for north bay. 1-σ bars are indicated. Perpendicular velocity component is negligible and omitted here. *C*, Same as figure 7.6*B* for central and south bay.

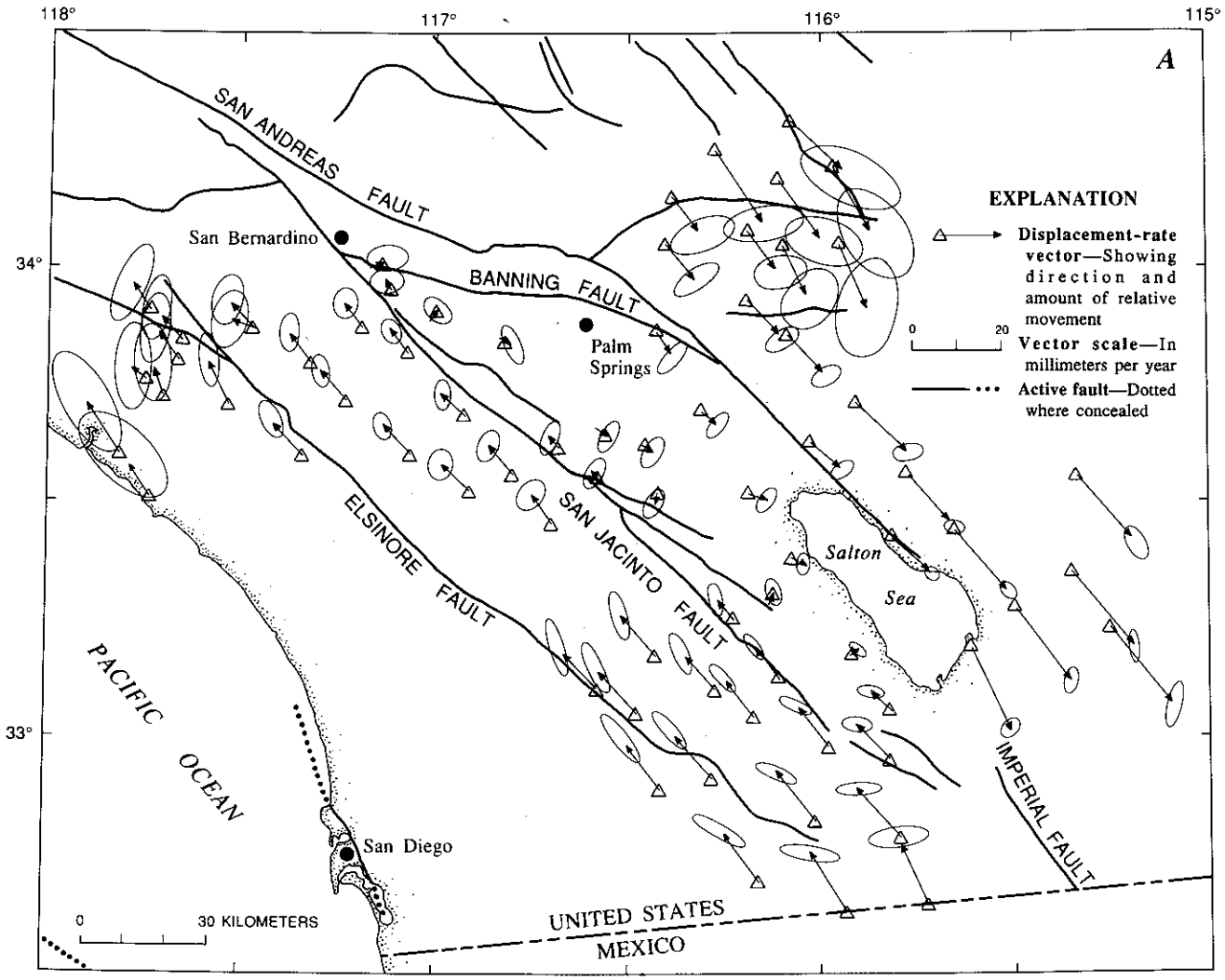

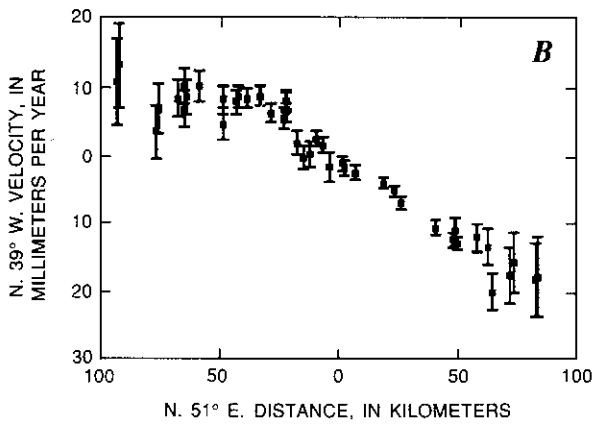

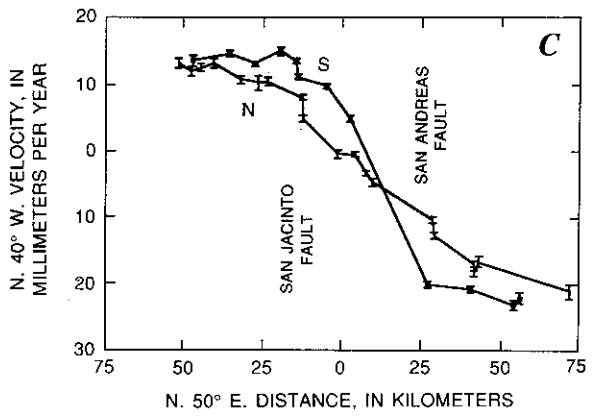

FIGURE 7.7.—Displacement rates in southern California. *A*, Relative right-lateral displacement rates determined from repeated geodetic-survey measurements during 1973–87. Error ellipses show 95-percent-confidence limits for each determination (Prescott and others, 1987). *B*, Relative station velocities parallel to approximate trend of the San Andreas fault (N. 39° W.) plotted against distance perpendicular to this trend, for stations in northern part of map in figure 7.7*A*. 1-σ error bars are indicated. Perpendicular velocity component is negligible and is not plotted here. *C*, Same as figure 7.7*B* for stations largely to north (N) and south (S) of the Salton Sea.

asthenosphere provide the dominant mechanism for interearthquake strain accumulation.

Note that in the context of these two models, the terms "lithosphere" and "asthenosphere" are linked to mechanical properties of the Earth's crust and upper mantle: The lithosphere is the strong elastic layer near the Earth's surface, and the asthenosphere is the region of ductile flow that lies beneath. Their boundary may thus lie well above the thermal boundary layer that separates the moving plates from the convecting mantle. If so, then at least the upper part of the "asthenosphere" forms part of the tectonic plate and moves with it.

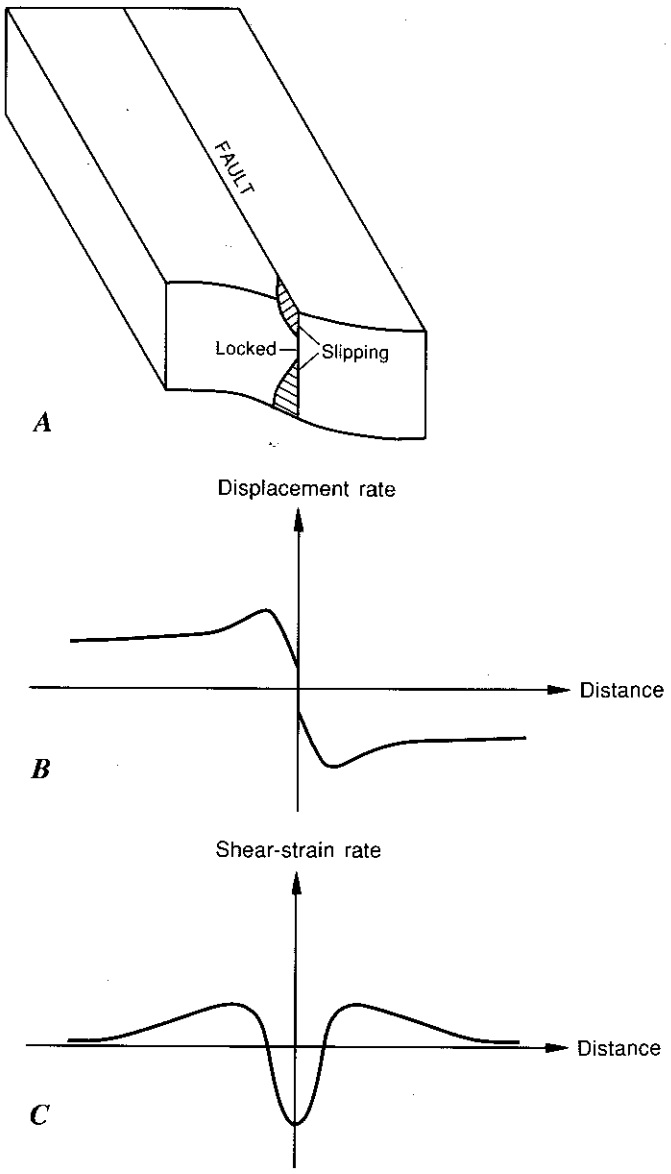

FIGURE 7.8.—Elastic-half-space model showing fault creep at surface, locked (nonslipping) fault at depth, and freely sliding zone at great depth (*A*). Displacement rate (*B*) and strain rate (*C*) are plotted against distance from fault.

Thus considered, the boundary between "lithosphere" and "asthenosphere" defines the zone of decoupling between surface tectonic processes and those that occur in the ductile region beneath. The location of this boundary is thus of central importance to the broad-scale tectonics of the San Andreas fault, the nature of the earthquake-generation process and its thermomechanical implications (see chap. 9), and the relation between shallow structural features and those inferred at depth (see chap. 8). I explore below the influence of this boundary location on cyclic earthquake-related deformation at the currently locked transform fault zones in the San Andreas, illustrating the contrasting mechanical behavior of the thick- and thin-lithosphere models.

All of the models considered here are two dimensional, and so neither slip nor mechanical properties vary along fault strike. Each model consists of only a single planar, vertical strike-slip fault. However, because the medium properties are linear elastic and (or) viscoelastic, the effects of multistranded fault zones can be obtained by simply superposing the deformation due to slip on individual fault segments. Furthermore, all of the two-dimensional models discussed here have also been considered in three dimensions, and so complexities arising from changes in fault strike, variations in slip along strike, and the finite extent of faulting can be incorporated straightforwardly as necessary. Similarly, except for the transition from elastic lithosphere to viscoelastic asthenosphere, depth variations in material properties are not considered, although, again, solutions have been obtained for faulting in plane-layered elastic

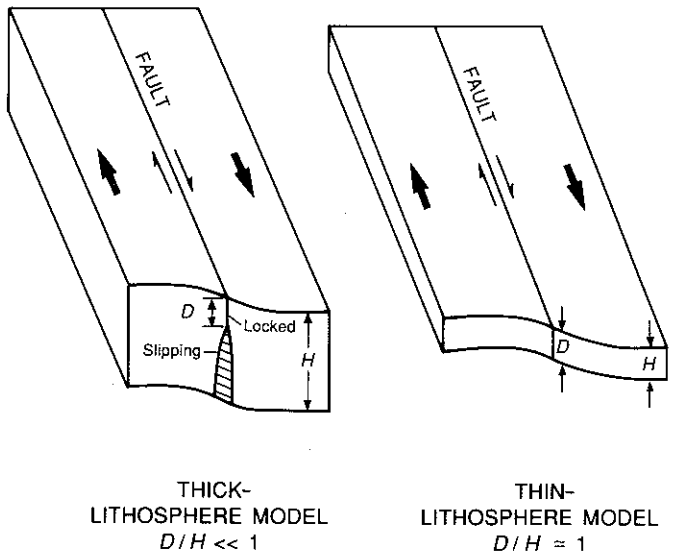

FIGURE 7.9.—Thick- and thin-lithosphere models. *D*, depth of coseismic faulting; *H*, thickness of elastically strong lithosphere. Small arrows along fault and larger arrows indicate direction of relative movement of fault and tectonic plates, respectively.

and viscoelastic media. Although fault end effects and changes in slip and geometry along fault strike can be locally important, these effects, as well as those due to depth-varying material properties, are generally second order relative to the deformation features described here. More important are the effects of the several subparallel strands that compose much of the San Andreas fault system along its two currently locked sections. In these sections, the interseismic deformation due to each major fault strand contributes significantly to the observed displacement pattern, and as a rule the effects of faults lying off the San Andreas proper cannot be safely ignored in matching models to data across the entire San Andreas boundary zone.

The simplest form of the thick lithosphere model, first proposed by Savage and Burford (1970), is illustrated in figure 7.10. In this idealized model, interearthquake strains accumulate uniformly throughout the deformation cycle and have precisely the same spatial pattern as coseismic strains, except that the sense of movement is reversed. The cycle consists of coseismic slip Δu extending from the surface to depth D and steady interearthquake aseismic slip at a constant rate $\dot{u}$ ($=\Delta u/T$, where T is the earthquake recurrence interval) beginning at $z=D$ and extending to great depth. For this model of interearthquake deformation, simple expressions relate surface-displacement rates $\dot{u}_x(y)$ and shear-strain rates $\dot{e}_{xy}(y)$ to the fault parameters $\dot{u}$ and D and the distance y from the fault trace:

$$\frac{du_x(y)}{dt} = \dot{u}_x(y) = \frac{\dot{u}}{\pi}\tan^{-1}\left(\frac{y}{D}\right)$$

and

$$\dot{e}_{xy}(y) = \frac{d}{dy}\left[\dot{u}_x(y)\right] = \frac{\dot{u}}{\pi D}\left[\frac{1}{1+\left(\frac{y}{D}\right)^2}\right]$$

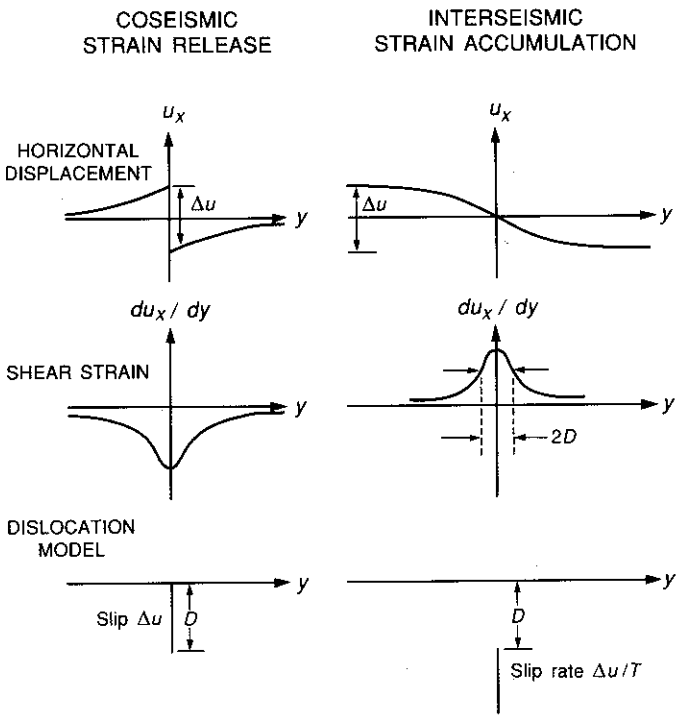

FIGURE 7.10.—Elastic-half-space model for earthquake cycle. Δu, coseismic slip; D, depth of coseismic slip; T, earthquake recurrence interval; u_x, horizontal displacement parallel to fault; du_x/dy, shear-strain component parallel to fault; y, distance from fault.

A principal utility of this model is the ease with which approximate values of displacement and strain rate can be computed, commonly as a preliminary step to more detailed computations that employ complex models which nonetheless show many of the same general features. For example, using typical San Andreas values of Δu=4 m, T=200 yr, and D=15 km, then $\dot{u}$=20 mm/yr, and the engineering shear-strain rate (twice the tensor strain rate $\dot{e}_{xy}$) at the fault trace (y=0) is about 0.8 μrad/yr, a value close to some of the peak strain rates plotted in figures 7.2 and 7.3. Furthermore, the bell-shaped distribution of secular strain across the model fault (middle right, fig. 7.10) generally accords with observations (fig. 7.3), and the width of the profile is a direct measure of the fault-locking depth D. (Note, however, that the observations summarized in figure 7.3 include strain rates determined from multistranded segments of the San Andreas fault system, and so they are not directly comparable to the model calculations for a single fault strand illustrated in fig. 7.10.) Recalling the observations discussed in the section above entitled "Observations of Crustal Deformation," the wider zone of secular strain across the southern section of the San Andreas can be rationalized if the depth of seismic slip and, thus, the locking depth of the fault are simply greater in southern than in northern California. As it stands, this model has no transient effects and so is too simple to explain the postearthquake strain changes plotted in figure 7.4. However, introducing a rather straightforward modification remedies this defect while accounting for the observed difference in strain-rate profiles between northern and southern California. Surprisingly, these same features are, for different reasons, natural consequences of the thin-lithosphere model.

The two models are illustrated in figure 7.11. In the thick-lithosphere model, postseismic effects are introduced by specifying transient postearthquake slip on a segment of the fault immediately beneath the coseismic rupture. Its time history is constrained by an exponentially decreasing slip rate (time constant α), and its magnitude by the requirement that the cumulative slip sum to the coseismic offset Δu by the end of the cycle. In the thin-lithosphere model, the transient deformation

results from flow in the asthenosphere due to stress relaxation after seismic faulting in the lithosphere. Its time scale is controlled by the asthenosphere-relaxation time $\tau=2\eta/\mu$, when η is the effective viscosity of the asthenosphere and μ is the average shear modulus of lithosphere and asthenosphere, here taken to be equal. In both models, the transient motions are superimposed on a steady component of deformation that is due to relative plate motion.

Detailed computations show that the two models produce surface deformations that with suitable choices of model parameters are observationally indistinguishable (see Thatcher, 1983). Here, the discussion is restricted to qualitative features, as summarized in figure 7.12. Near the fault, shear-strain rates monotonically decrease over time and gradually approach a constant (fig. 7.12*B*), while the deformation profile broadens and strains diffuse into the interiors of the adjacent plates as the cycle progresses (fig. 7.12*A*). It is easy to match the observed temporal decline in strain rate with either model; the particular parameter combinations are themselves not unique, and a range of choices can provide equally good agreement. All satisfactory thin-lithosphere models, however, require an elastic plate only 10 to 15 km thick, the maximum depth of coseismic slip in the 1906 earthquake (Thatcher, 1975). Both models predict a broadening of the zone of deformation that depends on the time interval since the latest great earthquake, and so the greater width of the strain-rate profile in southern California can be accounted for. For example, data from the northern, locked section of the San Andreas fault may correspond to times t_1 to t_3 in figure 7.12, whereas those from the southern section may correspond to times t_4 and t_5.

More complex models that combine features of both the thick- and thin-lithosphere models are also consistent with available data (for example, Li and Rice, 1987). Furthermore, coseismic and interearthquake fault slip undoubtedly vary as a function of depth, rather than abruptly terminating at some specified fault depth. Although this gradationality of the slip distribution modifies the detailed patterns of surface strain and displacement from those illustrated in figure 7.10, for example, the same qualitative features are preserved, and it will be difficult to distinguish between differing slip-depth distributions on the basis of surface-deformation measurements alone.

In summary, at transform plate boundaries, available data are consistent with both thick- and thin-lithosphere models but do not strongly constrain either. The most geophysically interesting feature of both models is the predicted postearthquake diffusion-like spread of strain from the plate-bounding fault into the interiors of the adjacent plates. Postearthquake surveys, however, are sufficiently infrequent and areal coverage sufficiently limited that these effects, if they indeed occur, have not been directly observed. Details of the temporal decline in deformation rate near the fault are also absent.

STRESS-SLIP-CONSTITUTIVE-LAW FAULT MODELS

A completely different class of large-scale-faulting models are now being developed to more realistically incorporate the fault-failure process into the earthquake deformation cycle (for example, Stuart, 1979; Tse and Rice, 1986). Instead of specifying slip on the plate-bounding fault, these models extrapolate from laboratory

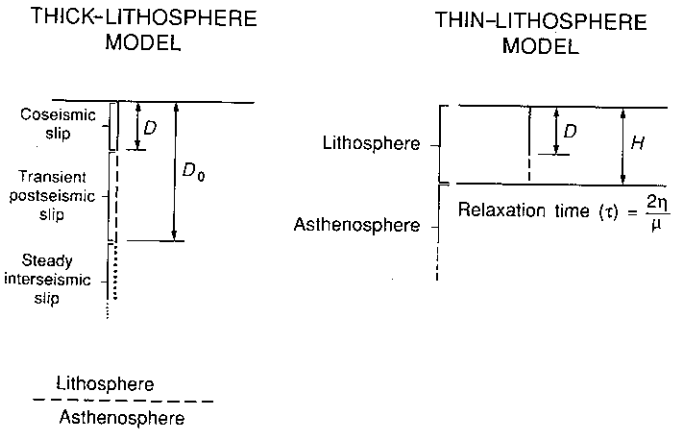

FIGURE 7.11.—Specific features of thick- and thin-lithosphere models. D, depth of coseismic slip; D_0, depth to bottom of zone of transient postseismic slip; H, thickness of elastically strong lithosphere; η, effective viscosity of asthenosphere; μ, average shear modulus of lithosphere and asthenosphere.

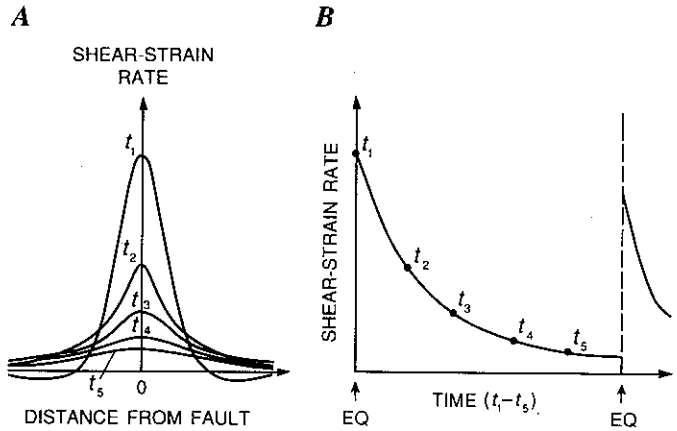

FIGURE 7.12.—Complete earthquake-cycle model predictions for thick- and thin-lithosphere models. *A*, Shear-strain rate versus distance from fault and its temporal evolution through deformation cycle. *B*, Shear-strain rate on fault versus time for one complete cycle. EQ, earthquake.

observations of the time-dependent frictional properties of rocks (for example, Dieterich, 1979; Tullis, 1988) to assign slip-stress-constitutive laws to the fault surface. As remotely applied stresses increase, each segment of the fault slips at a rate that depends on both the previous slip history and the current applied stress, and so the cycle of elastic-strain accumulation and release can be simulated. By specifying the depth dependence of fault frictional properties, a slip behavior nearly identical to that of the thick-lithosphere model (fig. 7.11*A*) follows naturally. A sample calculation of this type (Tse and Rice, 1986) illustrates the method and shows typical results (fig. 7.13). After a large coseismic slip event in approximately the upper 10 km of the model fault, transient postseismic slip occurs on both the coseismic fault plane and its downdip extension. As slip rates decline to near zero on the shallow segments of the fault, interseismic slip at greater depths approaches nearly steady-state values. Finally, near the end of the cycle, the constitutive model predicts an increase in slip rate on the shallow coseismic fault segment before the next large slip instability ("earthquake").

Although the appropriateness of this extrapolation of laboratory results to large-scale faulting is a matter of current debate and the scaling of laboratory parameters to the field is uncertain, Tse and Rice's calculations clearly demonstrate that the principal observed features of the earthquake deformation cycle on the San Andreas fault can be reproduced by such models. Ongoing laboratory studies should refine and modify the stress-slip-constitutive laws, and geodetic and continuous strain-monitoring observations of preearthquake and postearthquake crustal deformation can test the applicability of these postulates to large-scale faulting processes.

SUMMARY

Contemporary crustal movements in California are concentrated within a plate-boundary-deformation zone that is typically 50 to 200 km wide, approximately centered on the San Andreas fault. Integrated right-lateral displacement rates across this zone range from 33 to 37 mm/ yr, representing about 75 percent of the Pacific-North American relative plate motion. Most or all of the rest may be taken up east of the San Andreas fault system in the Basin and Range province. Although aseismic fault slip (creep) is a locally important component of this relative plate motion, most of the geodetically measured deformation represents elastic strain on the crustal blocks adjacent to faults of the San Andreas system. Rates of secular (interseismic) shear strain are a maximum on the two currently locked segments of the San Andreas fault, sites of the great 1857 and 1906

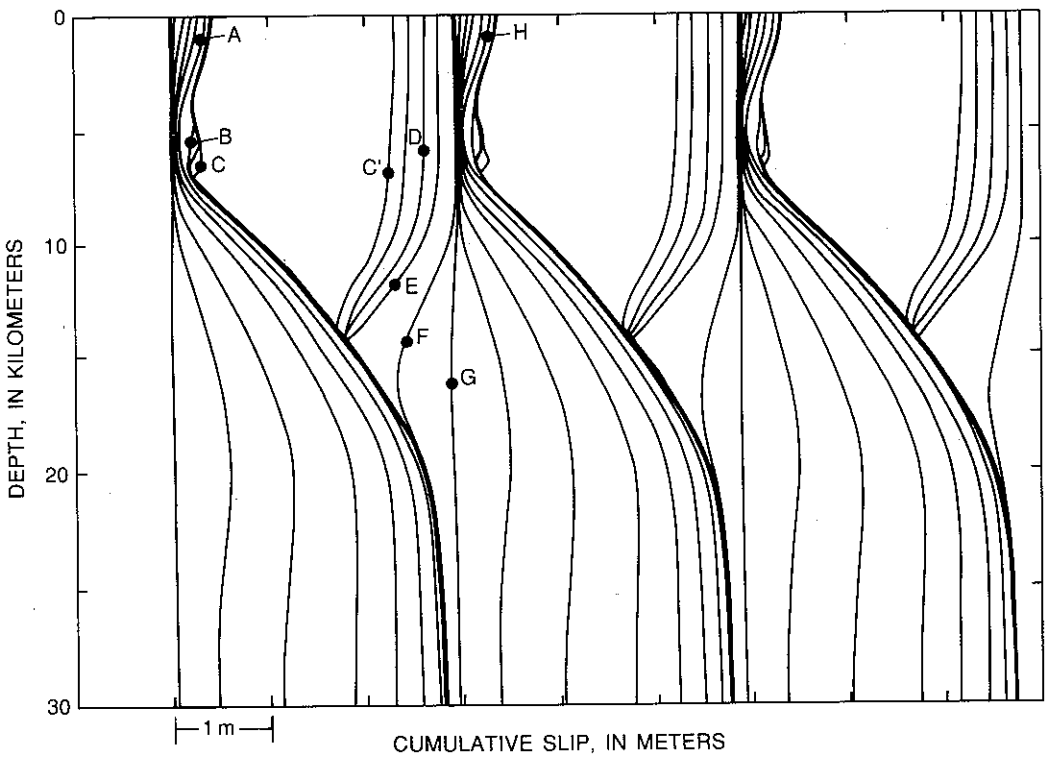

EXPLANATION

Location	Time interval
A to B	2.4 yr
B to C	4.6 hr
C to C'	Instantaneous
C' to D	4 s
D to E	3.5 min
E to F	77.8 days
F to G	3.6 yr
G to H	77.2 yr

$T = 83.8$ yrs

FIGURE 7.13.—Cumulative slip versus depth for selected time intervals through deformation cycle in quasi-static fault-instability model modified from Tse and Rice (1986). *T*, recurrence interval.

earthquakes. Values range from 0.4 to 0.6 parts per million per year (ppm/yr) at the fault to 0.1 ppm/yr 30 to 80 km from it. Deformation occurring at the times of large strike-slip earthquakes (coseismic strain) is concentrated within a few tens of kilometers of the surface fault rupture, indicating that earthquake fault slip is largely confined to the upper 10 to 15 km of the crust. After major events, postseismic shear strain occurs at transiently high rates (more than 2 ppm/yr) that decay to background interseismic rates over a time scale of years to tens of years.

Observations of coseismic, postseismic, and interseismic movements define the earthquake deformation cycle and constrain models of strain accumulation and release for strike-slip plate boundaries. Observations are fitted equally well by two contrasting models. In the first model, the depth of coseismic faulting is much less than the thickness of the elastically strong lithosphere, and postseismic and interseismic deformation result from transient and steady aseismic slip on the downward extension of the earthquake fault plane. At the other extreme, if earthquake slippage extends through most or all of the elastic lithosphere, interearthquake deformation is due to transient or steady flow in the underlying weak substrate ("asthenosphere").

FUTURE DIRECTIONS FOR RESEARCH

Although the broad outlines of current movement across the San Andreas boundary zone are now known and the main features of the cyclic deformation expected from great strike-slip earthquakes have been delineated, many issues still remain to be explored. Although all of the relative Pacific-North American plate motion occurring across California may have been measured geodetically, this determination is not yet definitive, and as much as 10 mm/yr of motion may be accommodated east or west of the approximately 100-km-wide zone defined by current measurements. Furthermore, the thickness of the elastically strong crust is uncertain by at least a factor of 3, and so major alternative models of the earthquake deformation cycle cannot be distinguished (fig. 7.9). Because surface-deformation observations cannot themselves resolve this ambiguity, other data, possibly gravity-field observations and lithospheric-deflection models (for example, McNutt, 1980), are needed.

Few details exist on the preseismic and postseismic movements related to large plate-boundary earthquakes. Whether detectably anomalous crustal movements precede large earthquakes is uncertain. Theoretical models and fragmentary observations suggest that precursory slip may occur on or beneath the eventual coseismic rupture plane. However, except for the observation that premonitory deformations must be small relative to coseismic movements (for example, Johnston and others, 1987), precursory slip is otherwise unconstrained. Existing data are sufficient to demonstrate that postseismic movements, at least those from great earthquakes, are large—commonly, 10 to 30 percent of the coseismic deformation (Thatcher, 1984)—but the time scale and spatial distribution of these motions are not well determined at strike-slip plate boundaries. Laboratory experiments on lower-crustal rock types suggest that their ductile behavior is not approximated well by linear viscoelasticity, as assumed in the thin-lithosphere model, but postseismic observations are not yet sufficiently detailed to confirm this expectation.

Furthermore, vertical crustal movements in California are not well understood. Though not dominant in California's largely strike-slip-faulting environment, vertical movements can nonetheless be locally important in such regions as the Los Angeles and Ventura Basins, the Transverse Ranges of southern California, and the Cape Mendocino area of northern California. Current and future work that integrates geologic and geodetic information in these regions should begin to shed light on long-term, secular vertical-movement patterns and their origins.

Within complex, multistranded fault zones and, possibly, in simpler regions, permanent inelastic deformation of upper-crustal rocks may contribute significantly to the current movement pattern. For example, at subduction boundaries, geologic and geodetic observations indicate a substantial imbalance between cumulative interearthquake strain and coseismic strain release, commonly reflected in long-term uplift or subsidence of coastal and inland regions. However, at such predominantly transcurrent boundaries as the San Andreas, the observable effects of inelastic strain are more subtle. The thermal consequences of such deformation may be the most direct evidence for inelastic strain (see chap. 9). However, for California at least, the available data are either contradictory or ambiguous, and the extent to which measured interearthquake movements release elastically stored strain is currently unresolved.

REFERENCES CITED

Bomford, Guy, 1980, Geodesy (4th ed.): London, Oxford University Press, 731 p.

Brace, W.F., and Byerlee, J.D., 1966, Stick-slip as a mechanism for earthquakes: Science, v. 153, no. 3739, p. 990–992.

Breen, N.A., Lisowski, Michael, and Prescott, W.H., 1987, Spatially varying patterns of crustal strain near the Mendocino triple junction, California [abs.]: Eos (American Geophysical Union Transactions), v. 68, no. 44, p. 1240.

Burford, R.O., and Harsh, P.W., 1980, Slip on the San Andreas fault in central California from alinement array surveys: Seismological

Society of America Bulletin, v. 70, no. 4, p. 1223–1261.
Castle, R.O., Church, J.P., Elliott, M.R., and Morrison, N.L., 1975, Vertical crustal movements preceding and accompanying the San Fernando earthquake of February 9, 1971: A summary: Tectonophysics, v. 29, p. 127–140.
DeMets, Charles, Gordon, R.G., Stein, Seth, and Argus, D.F., 1987, A revised estimate of Pacific-North America motion and implications for western North America plate boundary zone tectonics: Geophysical Research Letters, v. 14, no. 9, p. 911–914.
Dieterich, J.H., 1979, Modelling of rock friction, 1, Experimental results and constitutive equations: Journal of Geophysical Research, v. 84, no. B5, p. 2161–2168.
Johnston, M.J.S., Linde, A.T., Gladwin, M.T., and Borcherdt, R.D., 1987, Fault failure with moderate earthquakes: Tectonophysics, v. 144, no. 1–3, p. 189–206.
King, N.E., 1985, Horizontal deformation in the Mojave Desert near Barstow, California, 1979–1983: Journal of Geophysical Research, v. 90, no. B6, p. 4491–4494.
King, N.E., and Savage, J.C., 1983, Strain-rate profile across the Elsinore, San Jacinto and the San Andreas faults near Palm Springs, California, 1973–81: Geophysical Research Letters, v. 10, no. 1, p. 55–57.
—— 1984, Regional deformation near Palmdale, California, 1973–1983: Journal of Geophysical Research, v. 89, no. B4, p. 2471–2477.
Lajoie, K.R., 1986, Coastal tectonics, *in* Active tectonics: Washington, National Academy Press, p. 95–124.
Lawson, A.C., chairman, 1908, The California earthquake of April 18, 1906: Report of the State Earthquake Investigation Commission: Carnegie Institution of Washington Publication 87, 2 v.
Li, V.C., and Rice, J.R., 1987, Crustal deformation in great California earthquake cycles: Journal of Geophysical Research, v. 92, no. B11, p. 11533–11551.
Lisowski, Michael, and Prescott, W.H., 1981, Short-range distance measurements along the San Andreas fault system in central California, 1975 to 1979: Seismological Society of America Bulletin, v. 71, no. 5, p. 1607–1624.
Louie, J.N., Allen, C.R., Johnson, D.C., Haase, P.C., and Cohn, S.N., 1985, Fault slip in southern California: Seismological Society of America Bulletin, v. 75, no. 3, p. 811–833.
McNutt, Marcia, 1980, Implications of regional gravity for state of stress in the earth's crust and upper mantle: Journal of Geophysical Research, v. 85, no. B11, p. 6377–6396.
Minster, J.B., and Jordan, T.H., 1987, Vector constraints on Western U.S. deformation from space geodesy, neotectonics, and plate motions: Journal of Geophysical Research, v. 92, no. B6, p. 4798–4804.
Prescott, W.H., 1976, An extension of Frank's method for obtaining crustal shear strains from survey data: Seismological Society of America Bulletin, v. 66, no. 6, p. 1847–1853.
—— 1981, The determination of displacement files from geodetic data along a strike slip fault: Journal of Geophysical REsearch, v. 86, no. B7, p. 6067–6072.
—— 1985, An overview of the distribution of relative plate motion along the San Andreas fault system from Hollister, California, to the Mendocino triple junction, *in* Shearer, C.F., Minutes of the National Earthquake Prediction Evaluation Council, July 26–27, 1985, Menlo Park, California: U.S. Geological Survey Open-File Report 85–754, p. 232–246.
Prescott, W.H., and Lisowski, Michael, 1983, Strain accumulation along the San Andreas fault system east of San Francisco Bay, California: Tectonophysics, v. 97, no. 1–4, p. 41–56.
Prescott, W.H., Lisowski, Michael, and Savage, J.C., 1981, Geodetic measurement of crustal deformation on the San Andreas, Hayward, and Calaveras faults near San Francisco, California: Journal of Geophysical Research, v. 86, no. B11, p. 10853–10869.
—— 1987, Velocity field along the San Andreas fault in southern California [abs.]: Eos (American Geophysical Union Transactions), v. 68, no. 44, p. 1506.
Prescott, W.H., and Yu, S.-B., 1986, Geodetic measurements of horizontal deformation in the northern San Francisco Bay region, California: Journal of Geophysical Research, v. 91, no. B7, p. 7475–7484.
Sauber, Jeanne, Thatcher, Wayne, and Solomon, S.C., 1986, Geodetic measurement of deformation in the central Mojave Desert, California: Journal of Geophysical Research, v. 91, no. B12, p. 12683–12693.
Savage, J.C., and Burford, R.O., 1970, Accumulation of tectonic strain in California: Seismological Society of America Bulletin, v. 60, no. 6, p. 1877–1896.
Savage, J.C., and Lisowski, Michael, 1980, Deformation in Owens Valley, California: Seismological Society of America Bulletin, v. 70, no. 4, p. 1225–1232.
—— 1984, Deformation in the White Mountain seismic gap, California-Nevada, 1972–1982: Journal of Geophysical Research, v. 89, no. B9, p. 7671–7687.
Savage, J.C., and Prescott, W.H., 1973, Precision of geodolite distance measurements for determining fault movements: Journal of Geophysical Research, v. 78, v. 26, p. 6001–6008.
Savage, J.C., Prescott, W.H., and Gu, Guohua, 1986, Strain accumulation in southern California 1973–1984: Journal of Geophysical Research, v. 91, no. B7, p. 7455–7473.
Savage, J.C., Prescott, W.H., Lisowski, Michael, and King, N.E., 1979, Geodolite measurements of deformation near Hollister, California, 1971–1978: Journal of Geophysical Research, v. 84, no. B13, p. 7599–7615.
—— 1981, Strain accumulation in southern California, 1973–1980: Journal of Geophysical Research, v. 86, no. B8, p. 6991–7001.
Schulz, S.S., Mavko, G.M., Burford, R.O., and Stuart, W.D., 1982, Long-term fault creep observations in central California: Journal of Geophysical Research, v. 87, no. B8, p. 6977–6982.
Segall, Paul, and Harris, R.A., 1987, Earthquake deformation cycle on the San Andreas fault near Parkfield, California: Journal of Geophysical Research, v. 92, no. B10, p. 10511–10525.
Sibson, R.H., 1982, Fault zone models, heat flow, and the depth distribution of earthquakes in the continental crust of the United States: Seismological Society of America Bulletin, v. 72, no. 1, p. 151–163.
Stein, R.S., 1983, Reverse slip on a buried fault during the 2 May 1983 Coalinga earthquake: Evidence from geodetic elevation changes, in Bennett, J.H., and Sherburne, R.W., eds., The 1983 Coalinga, California earthquakes: California Division of Mines and Geology Special Publication 66, p. 151–163.
Stein, R.S., and Thatcher, Wayne, 1981, Seismic and aseismic deformation associated with the 1952 Kern County, California, earthquake and relationship to the Quaternary history of the White Wolf fault: Journal of Geophysical Research, v. 86, no. B6, p. 4913–4928.
Stuart, W.D., 1979, Strain softening prior to two-dimensional strike slip earthquakes: Journal of Geophysical Research, v. 84, no. B3, p. 1063–1070.
Thatcher, Wayne, 1975, Strain accumulation and release mechanism of the 1906 San Francisco earthquake: Journal of Geophysical Research, v. 80, no. 35, p. 4862–4872.
—— 1979, Systematic inversion of geodetic data in central California: Journal of Geophysical Research, v. 84, no. B5, p. 2283–2295.
—— 1983, Nonlinear strain buildup and the earthquake cycle on the San Andreas fault: Journal of Geophysical Research, v. 88, no. B7, p. 5893–5902.
Tse, S.T., and Rice, J.R., 1986, Crustal earthquake instability in

relation to the depth variation of frictional slip properties: Journal of Geophysical Research, v. 91, no. B9, p. 9452–9472.

Tullis, T.E., 1988, Rock friction constitutive behavior from laboratory experiments and its implications for an earthquake prediction field monitoring program: Pure and Applied Geophysics, v. 126, no. 2–4, p. 555–588..

Yeats, R.S., 1977, High rates of vertical crustal movement near Ventura, California: Science, v. 196, no. 4287, p. 295–298.

Zhang, Y., Thatcher, Wayne, and Snay, R.A., 1988, Coseismic slip in the 1940 and 1979 Imperial Valley earthquakes and its implications [abs.]: Eos (American Geophysical Union Transactions), v. 69, p. 1433.